

Hybrid Silicon Photonic – Lithium Niobate Electro-Optic

Mach-Zehnder Modulator Beyond 100 GHz

Peter O. Weigel^{1,*}, Jie Zhao¹, Kelvin Fang¹, Hasan Al-Rubaye¹, Douglas Trotter², Dana Hood², John Mudrick², Christina Dallo², Andrew T. Pomerene², Andrew L. Starbuck², Christopher T. DeRose², Anthony L. Lentine², Gabriel Rebeiz¹ and Shayan Mookherjea^{1,*}

¹ University of California, San Diego, Electrical & Computer Engineering, La Jolla, California 92093-0407, USA

² Sandia National Laboratories, Applied Microphotonic Systems, Albuquerque, New Mexico, 87185, USA

* Correspondence to: pweigel@eng.ucsd.edu, smookherjea@ucsd.edu

Advances in silicon (Si) photonics have resulted in phase (depletion mode) electro-optic modulators (EOMs) with an electrical 3-dB bandwidth up to 50 GHz [1], but to achieve higher bandwidths, different materials and physical phenomena are used. Lithium Niobate (LN) Mach-Zehnder modulators (MZM), while being the traditional EOM platform [2], have not yet demonstrated DC-to-beyond-100-GHz electrical bandwidths. We demonstrate a hybrid LN-Si MZM which achieves 102 GHz 3-dB electrical bandwidth; this EOM exceeds the bandwidth of the highest-speed bulk LN MZM previously reported [3] by 32 GHz, with $V_{\pi}L=6.6$ V.cm being more than 50% lower. Our design allows compatibility with silicon photonics, with light input/output and optical components, including directional couplers, low-radius bends, and path-length difference segments, realized in a foundry Si photonics process [4]. An un-patterned thin-film of LN was simply bonded to the patterned Si waveguide circuits. Such a device can bring ultrawide electro-optic bandwidths to integrated silicon photonics, and benefit applications in analog and digital communications, millimeter-

wave instrumentation, analog-to-digital conversion, sensing, antenna remoting and phased arrays.

LN is a suitable material for high-bandwidth electro-optic modulation, with stand-alone Mach-Zehnder modulator (MZM) devices having reached 110 GHz optical (70 GHz electrical) 3-dB bandwidth about two decades ago (in an unpackaged device) [3]. As a step towards integrated modulators, a variety of approaches using thin-film LN [5, 6] have been reported [7, 8, 9, 10, 11]. The ability to match the optical and microwave indices by varying the dimensions of the LN layer and the rib loading Si waveguide offer new opportunities to achieve true optical-RF phase matching to very high frequencies without artificial velocity matching structures, and indeed, electro-optic modulation sidebands have been measured to several hundred gigahertz (though not the 3-dB point) [12].

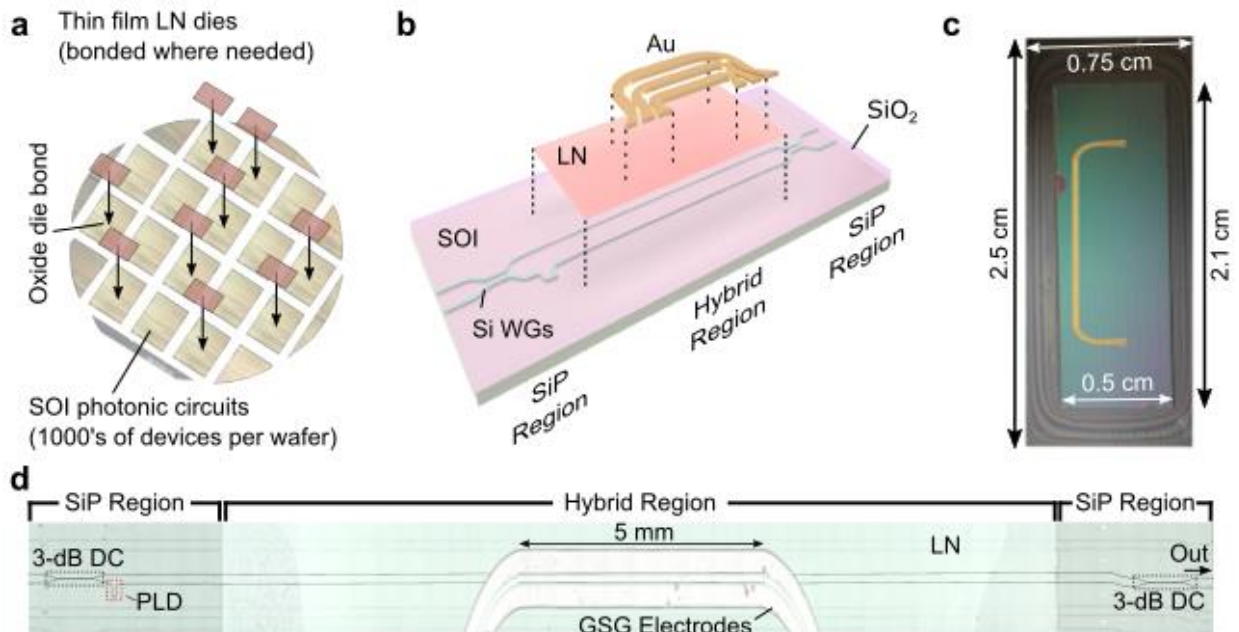


Fig. 1a, Thin film x-cut lithium-niobate (LN) on insulator dies were bonded at room temperature to segmented dies of a patterned and planarized silicon-on-insulator (SOI) wafer which contained fabricated silicon photonic

waveguide circuits. No etching or patterning of the LN film was performed. **b**, Exploded representation of the EOM, where an unpatterned, un-etched LN thin film was bonded to a Mach-Zehnder interferometer fabricated in Si. Gold electrodes were deposited and electroplated directly on the LN film. 'SiP Region' denotes the SiO₂-clad region outside the bonded LN film, containing Si waveguide circuits, such as feeder waveguides, bends, directional couplers, and path-length difference segments. **c**, Top view of a representative fabricated hybrid Si-LN EOM test chip, which contains 60 EOM waveguide structures in parallel (in the north-south direction); for this report, test electrodes for use in push-pull configuration were only fabricated on one EOM device. **d**, Composite microscope image of the EOM. DC: directional coupler, PLD: path-length difference, GSG: ground-signal-ground, SiP: Si photonics.

In our fabrication approach, depicted in Fig. 1, MZM's were built on a silicon photonics platform, using photolithography on silicon-on-insulator wafers (220 nm Si thickness, 3 μm oxide thickness) and did not require sub-resolution features unlike most plasmonic or polymeric slot modulators [13, 14]. Silicon thinning (down to 150 nm) and feature patterning were followed by oxide deposition and subsequent chemical mechanical polishing and oxide thinning by a timed wet etch (diluted hydrofluoric acid) process. After die segmentation, commercially-procured x-cut thin-film LN on insulator (NanoLN, Jinan Jingzheng Electronics Co. Ltd.) was bonded over a large area (~1 cm²), but not processed further (e.g., no etching [9, 15] or sawing [16] of LN was performed). Oxide bonding was done at room temperature after surface cleaning and surface plasma activation steps. The bonded sample was thermally annealed at 200°C for one hour under pressure. The bonded stack has been shown to withstand repeated temperature-cycling to at least 300°C [17], sufficient for the post-processing required here. The LN die handle was removed, followed by coplanar waveguide electrode formation using gold electroplating. A fully fabricated chip is shown in Fig. 1c; a microscope image of the EOM is provided in Fig. 1d. The electrodes used

here are less than one-third the height used in Ref. [3]. The Si photonics wafer fabrication was performed at Sandia; the other fabrication steps and measurements were performed at UCSD. The resulting device is on a Si handle, potentially mitigating piezoelectric resonances from traditional LN substrates [18], and can be integrated with additional photonics components. As described below, the optical input and output from the MZM section were through (crystalline) silicon photonic waveguiding structures.

For the MZM reported here, the silicon photonics region outside the bonded LN area included four types of optical waveguide structures: fully-etched tapers for light input and output from the chip (edge couplers), single-mode broadband directional couplers (>15 dB extinction ratio from 1525-1575 nm, maximum of approximately 25 dB), path-length difference (PLD) segment (including spline curve bends), and adiabatic waveguide tapers for inter-layer transitions (Si-to-LN and vice-versa). Precise foundry processing of the Si photonic features results in accurate and repeatable formation of the directional coupler splitting ratio. Since the LN layer is neither patterned nor etched in our design, there was no alignment issue at the bonding step; the Si features alone determine the optical propagation path.

The adiabatic waveguide tapers were designed to achieve a vertical inter-layer transition (from Si to LN, and the reverse). As shown in Fig. 2, the design uses the TE-polarized fundamental guided mode, which is also used in conventional silicon photonics at 1.5 μm wavelengths [19]. Since the refractive index of Si at these wavelengths (approximately 3.5) is significantly higher than that of LN (approximately 2.2), the large index difference enables

control of the mode size and location (i.e., mainly in the Si rib or the LN slab) through lithography of the Si layer alone. Thus, only the width of the Si waveguide (w) was varied in our design; when $w > 600$ nm, light at $1.55 \mu\text{m}$ is mostly confined within the Si rib with confinement factor $\Gamma_{\text{Si}} = 64\%$ (Mode A) and $\Gamma_{\text{Si}} = 58\%$ (Mode B). For $w = 320$ nm, light is guided in Mode C and “sees” the LN slab layer, with confinement fraction in the LN layer calculated as $\Gamma_{\text{LN}} = 81\%$ and $\Gamma_{\text{Si}} = 5\%$. Longitudinal Poynting vector simulations of these modes are shown in Fig. 2c. The Mode B – Mode C transition loss is estimated as 0.1 dB from simulations and is described in more detail in previous work [20]. A benefit of these high-bandwidth modulators is that Γ_{LN} has less variation with small errors in fabricated waveguide dimensions than plasmonic or polymeric slot waveguide MZMs.

Vertical, inter-layer transitions to and from the hybrid LN-Si region occur only where needed, inside the perimeter of the bonded region. Optical losses between Modes A and B are minimized by keeping the Si waveguide wide ($w = 650$ nm) when crossing into the hybrid region. Thus, the edges of the bonded thin film, even if rough, do not significantly affect propagation. Complex waveguiding circuits can be built up with multiple vertical transitions if desired, as shown elsewhere [20], but were not required here. A design library of hybrid LN-Si components has been created to aid in simulations and design within the Lumerical Interconnect simulation environment [21].

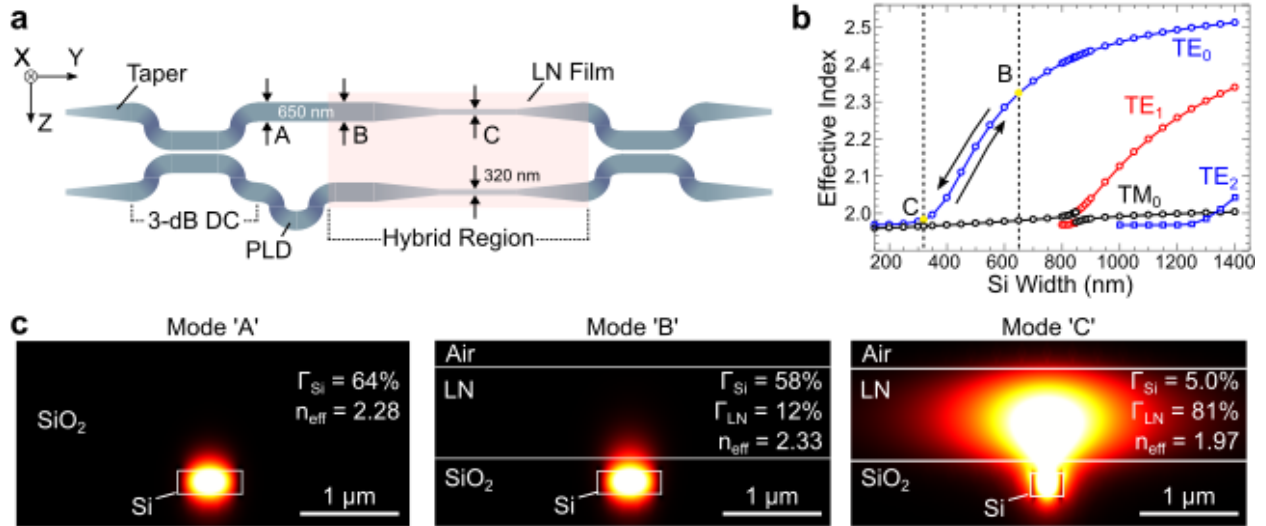


Fig. 2a, Schematic of the EOM (not to scale, not showing electrodes), including two 3-dB directional couplers (DC) and a waveguide segment for path-length difference (PLD). Three optical waveguide modes are used, labeled as A, B, and C. Modes A (Si under SiO₂) and B (Si under LN) have Si rib width $w = 650$ nm whereas mode C has $w = 320$ nm. **b**, Dispersion curves (effective index versus w) in the hybrid region; w values for modes B and C are chosen to stay within the single-mode region of operation. An adiabatic waveguide transition (variation in w) is designed to evolve from mode B to C and vice versa. **c**, Calculated Poynting vector components along the direction of propagation. Modes A and B are Si-guided and have a similar confinement fraction in Si. Mode C, with LN confinement factor (Γ_{LN}) greater than 80%, is used in the phase-shifter segments.

Light input and output were achieved using tapered single-mode, polarization-maintaining fibers, whose positions were controlled using micro-positioning stages. From test structures, an optical propagation loss of -0.6 dB/cm in the hybrid LN-Si region was measured. The propagation losses in the Si-only regions were about 1.3 dB/cm and are kept short in this design. The edges of the silicon photonic chip were lightly polished, but not fully prepared or packaged; hence, the edge coupling loss was about -3 dB per edge and the total fiber-to-fiber insertion loss was -13.8 dB. The calculated intrinsic loss of the full MZM (not including

edge couplers), based on the measured propagation loss (-0.6 dB/cm) and the device length (0.5 cm), and simulated inter-layer transition loss estimates (-0.1 dB each) should be about -0.7 dB. However, the actual insertion loss was about -7.8 dB, 2.6 dB of which came from metallization, measured from a comparison of a passive (interferometer) and active (modulator) structure. The excess 2.6 dB loss is most likely due to unoptimized bends in the electrical lines, which pass directly over the optical mode. At low speeds, the MZM demonstrated a high extinction ratio (> 20 dB) as shown in Fig. 3a, with $V_{\pi}L = 6.6$ V.cm for an $L=0.5$ cm device.

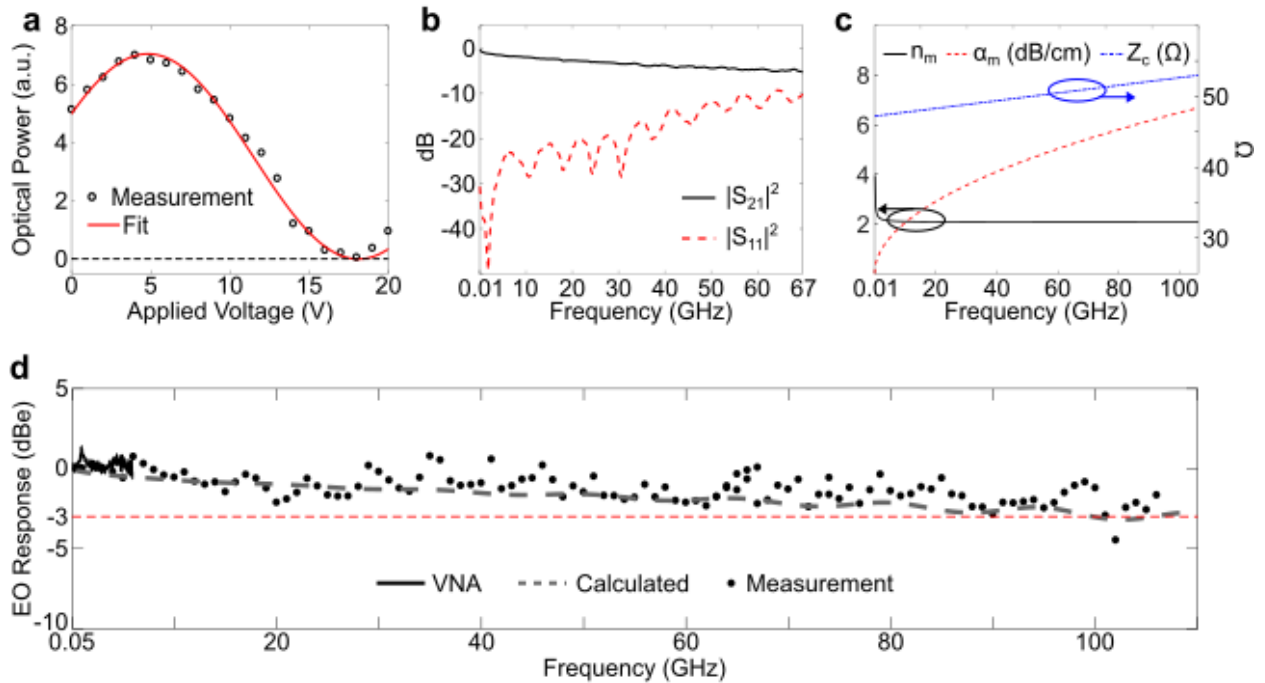


Fig. 3a, Optical transmission (arbitrary units, proportional to milliwatts) versus dc voltage. Fitted $V_{\pi}L = 6.6$ V.cm at $1.565 \mu\text{m}$; device length $L = 0.5$ cm. **b**, Measured electrical S-parameters of the MZM's coplanar-waveguide transmission line. **c**, Left y-axis: extracted microwave phase index n_m and loss α_m (dB/cm). Right y-axis: characteristic impedance Z_c (Ω). **d**, Electro-optic response of the EOM. Solid black line: VNA; dashed

gray line: calculated response from electrical S-parameters of **c**; black circles: electro-optic response from sideband OSA measurements.

RF measurements were performed on a bare-die chip using 50-Ω probes rated to 110 GHz and using laboratory equipment and RF waveguide components also rated and calibrated to about 110 GHz. The RF driving waveform was either from an RF oscillator (up to 67 GHz) or frequency multipliers (up to 106 GHz). GSG probes were used for both launch and termination. Calibration of the signal pathway was performed using a high-frequency RF power sensor. To inform a computational model of the expected behavior, electrical S-parameters were measured using a Vector Network Analyzer up to 67 GHz, as shown in Fig. 3b. From standard algebraic transformations and lossy transmission line circuit analysis [22], the microwave index (n_m), loss (α_m), and characteristic impedance (Z_c) were calculated, fitted, and extrapolated to higher frequencies, as shown in Fig. 3c. n_m was fitted to a power equation and Z_c was fitted to a first-order polynomial. Because α_m is dominated by conductor losses, it was fitted to a polynomial proportional to $f^{1/2}$. From that fit, $\alpha_m = 0.65 \text{ dB}\cdot\text{cm}^{-1}\cdot\text{GHz}^{1/2}$, and $n_m = 2.1$ without significant variation over the relevant frequency range. Z_c also varies only marginally with frequency, with a mean value of 49 Ω.

The small-signal optical modulation response of an electro-optic Mach-Zehnder modulator based on phase modulation (a good approximation of the Pockels effect in LN) is [23]:

$$m(\omega) = \frac{R_L + R_G}{R_L} \left| \frac{Z_{in}}{Z_{in} + Z_G} \right| \left| \frac{(Z_L + Z_0)F_{u+} + (Z_L - Z_0)F_{u-}}{(Z_L + Z_0) \exp(\gamma_m L) + (Z_L - Z_0) \exp(-\gamma_m L)} \right| \quad (1)$$

where n_o is the optical group index, n_m and α_m are the microwave index and loss coefficient, L is the phase-shifter arm length, ω is the RF frequency, c is the speed of light, Z_L (R_L) and Z_G (R_G) are the load and generator impedances (resistances), Z_0 is the electrode (transmission line) characteristic impedance, Z_{in} is the RF line input impedance, and using the definitions $F(u) = [1 - \exp(u)]/u$; $u_{\pm} = \pm \alpha_m L + j(\omega/c) [\pm n_m - n_o]L$; and complex RF propagation constant $\gamma_m = \alpha_m + j \omega n_m/c$.

Equation (1) is a low-pass filter type response, whose 3-dB (electrical roll-off) frequency ($f_{3dB,el}$) is maximized by matching of the optical and RF indices, matching the load and generator impedances, and minimizing the RF loss, but is not affected by the optical propagation loss. Lower optical propagation loss (α_{opt}) improves overall transmission, but for values of $\alpha_{opt} < 1$ dB/cm and device lengths < 1 cm, the actual measured losses are dominated by non-idealities, such as imperfect chip coupling, or non-unitary power splitting at directional couplers, and further optical loss reduction plays only a minor role.

The implications of equation (1) can be understood by assessing its behavior with regard to each significant parameter in turn. Assuming velocity and impedance matching, the RF-loss limited bandwidth results in a 3-dB point of $\alpha_m(f_{3dB,el}).L = 6.4$ dB. Using $L = 0.5$ cm for the device under test, and requiring the 3-dB electrical frequency $f_{3dB,el} \geq 100$ GHz, we need $\alpha_m(100 \text{ GHz}) \leq 4 \text{ dB.cm}^{-1}$ assuming $f^{1/2}$ scaling of the loss. As shown in Fig. 3, measurements showed $\alpha_m(10 \text{ GHz}) = 2 \text{ dB.cm}^{-1}$, well under the limit, and thus, RF losses are not a limitation. Assuming impedance matching and no RF loss, the bandwidth limitation $f_{3dB,el}.L = (0.13/\Delta n)$ GHz.m, where $\Delta n = n_m - n_o$. Thus, achieving $f_{3dB,el} \geq 100$ GHz for a 0.5 cm long device requires

$\Delta n_{m0} = n_m - n_0 \leq 0.26$. Calculations for our device indicate that $\Delta n_{m0} \approx 0.22$, which is under the threshold for achieving 100 GHz electrical bandwidth. Moreover, the electrode length times bandwidth product [24] “LB” = $c/\Delta n = 136$ GHz.cm (i.e., zero modulation response at $f = 136$ GHz for a 1 cm long device) whereas the fabricated device which achieves 102 GHz modulation has $L = 0.5$ cm, a factor of two shorter. Thus, neither RF losses nor index matching are fundamental limitations, as they have been in the past.

The method of Ref. [25] was used to detect signals and modulation sidebands at an optical wavelength of 1565 nm. With the modulator biased at quadrature, the difference (log scale) between the optical intensity of the first sideband and carrier signal was used to extract the modulation index, and thus the frequency response from 106 GHz down to 0.8 GHz (providing a safe margin for the 0.18 GHz resolution of the OSA). The peak-to-peak RF drive amplitude was about 0.6 Volts. Frequency multipliers were used for the frequency range above 67 GHz up to 106 GHz. Confirmation, and additional extension to lower frequencies, was provided by measuring the response of the device using a low-frequency VNA (50 MHz to 6 GHz) with an optical photodetector. The electro-optic response is shown in Fig. 3d, and an (electrical) 3-dB bandwidth was observed to lie at 102 GHz. We believe the minor ripples shown in the measured data are related to imperfect impedance matching (between Z_L , Z_G and Z_0), which can be improved with fabrication iterations. The measurement matches well with the calculated response (dashed black line in Fig. 3d), which was obtained by plugging the measured values of Fig. 3c into Eq. (1). Some of the scatter in the measurements at the highest frequencies arises from the calibration of the frequency extenders, which have nonlinear and discontinuous dispersion curves. The measured flat-spectrum modulation

response is consistent with our simulation based on electrical S-parameter measurements, which predicts flat frequency response to even higher frequencies.

Taken together, both theory and measurements support the performance of this device as a greater-than-100-GHz electrical bandwidth EOM. However, there are some areas of planned future improvements. Firstly, the bonding process relies on smooth oxide layers. Oxide thicknesses that are not optimal will reduce EOM performance, due to poor modulation efficiency or increased optical loss due to optical mode overlap with electrodes. While this does not affect our current die-bonding approach, in which we select which dies to attempt to bond, a more scalable wafer-to-wafer bonding approach may require further planarization process improvements. Secondly, electro-optic measurements at frequencies beyond 67 GHz require RF multipliers and time-consuming calibrations using appropriate waveguides, cables, probes and detectors for each frequency band, as observed elsewhere [26]. Packaging for field implementations incurs challenges: the 70-GHz unpackaged LN modulator of Ref. [3] achieved a 3-dB bandwidth, when packaged, of only about 30 GHz [27], which highlights the challenges in designing low-loss feed structures and other technical aspects. Finally, the product $V_{\pi}L = 6.6 \text{ V}\cdot\text{cm}$ (with a 0.5 cm device) in our best-performing device compares favorably with commercial technology, but the present devices were not designed to minimize $V_{\pi}L$. An order-of-magnitude lower $V_{\pi}L$ product can be achieved using plasmonic [28] or graphene [29] modulators, which are less widely adopted than LN modulators at this time.

In summary, we report an electro-optic Mach Zehnder modulator (MZM) based on single-mode silicon (Si) photonic waveguides bonded to a thin film of lithium niobate (LN), thus utilizing the well-known Pockels electro-optic effect, which has been shown, twenty years ago, to scale up to the previous record 70 GHz electrical 3-dB bandwidth in bulk LN modulators [3]. We report a 3-dB electrical bandwidth of 102 GHz, and the product $V_{\pi}L = 6.6$ V.cm is a 54% reduction from Ref. [3]. The input and output are in silicon photonics, and the fabrication process, which does not require etching or sawing of LN, is based on a standard silicon photonics foundry fabrication flow. Such modulators can break the limits of current-generation electro-optic modulators used in silicon photonics and allow integrated silicon photonics to scale to much higher bandwidths.

References:

- [1] J. Sun, M. Sakib, J. Driscoll, R. Kumar, H. Jayatilleka, Y. Chetrit and H. Rong, *A 128 Gb/s PAM4 Silicon Microring Modulator*, San Diego, CA, 2018, paper Th4A.7.
- [2] E. L. Wooten, K. M. Kissa, A. Yi-Yan, E. J. Murphy, D. A. Lafaw, P. F. Hallemeier, D. Maack, D. V. Attanasio, D. J. Fritz, G. J. McBrien and D. E. Bossi, "A Review of Lithium Niobate Modulators for Fiber-Optic Communications Systems," *IEEE Journal of Selected Topics in Quantum Electronics*, 2000.
- [3] K. Noguchi, O. Mitomi and H. Miyazawa, "Millimeter-Wave Ti:LiNbO₃ Optical Modulators," *Journal of Lightwave Technology*, vol. 16, no. 4, pp. 615-619, 1998.
- [4] C. T. DeRose, M. Gehl, C. Long, N. Boynton, N. Martinez, A. Pomerene, A. Starbuck, C. Dallo, D. Hood, D. C. Trotter, P. Davids and A. Lentine, "Radio frequency silicon photonics at Sandia National Laboratories," in *2016 IEEE Avionics and Vehicle Fiber-Optics and Photonics Conference (AVFOP)*, Long Beach, CA, 2016.

- [5] M. Levy, R. M. Osgood Jr., R. Liu, L. E. Cross, G. S. Cargill III, A. Kumar and H. Bakhru, "Fabrication of single-crystal lithium niobate by crystal ion slicing," *Applied Physics Letters*, vol. 73, pp. 2293-2295, 1998.
- [6] G. Poberaj, H. Hu, W. Sohler and P. Gunter, "Lithium niobate on insulator (LNOI) for micro-phonic devices," *Laser Photonics Review*, vol. 6, pp. 488-503, 2012.
- [7] L. Chen, J. Chen, J. Nagy and R. M. Reano, "Highly linear ring modulator from hybrid silicon and lithium niobate," *Optics Express*, vol. 23, pp. 13255-13264, 2015.
- [8] A. Rao, A. Patil, P. Rabiei, A. Honardoost, R. DeSalvo, A. Paoletta and S. Fathpour, "High-performance and linear thin-film lithium niobate Mach-Zehnder modulators on silicon up to 50 GHz," *Optics Letters*, vol. 41, no. 24, pp. 5700-5703, 2016.
- [9] A. J. Mercante, P. Yao, S. Shi, G. Schneider, J. Murakowski and D. W. Prather, "110 GHz CMOS Compatible thin film LiNbO₃ modulator on silicon," *Optics Express*, vol. 24, no. 14, pp. 15590-15595, 2016.
- [10] C. Wang, M. Zhang, B. Stern, M. Lipson and M. Loncar, "Nanophotonic lithium niobate electro-optic modulators," *Optics Express*, vol. 26, no. 2, pp. 1547-1555, 2018.
- [11] L. Chen, Q. Xu, M. G. Wood and R. M. Reano, "Hybrid silicon and lithium niobate electro-optical ring modulator," *Optica*, vol. 1, no. 2, pp. 112-118, 2014.
- [12] J. Macario, P. Yao, S. Shi, A. Zabolocki, C. Harrity, R. D. Martin, C. A. Schuetz and D. W. Prather, "Full spectrum millimeter-wave modulation," *Optics Express*, vol. 20, pp. 23623-23629, 2012.
- [13] S. Zhu, G. Q. Lo and D. L. Kwong, "Phase modulation in horizontal metal-insulator-silicon-insulator-metal plasmonic waveguides," *Optics Express*, vol. 21, pp. 8320-8330, 2013.

- [14] M. Ayata, Y. Fedoryshyn, W. Heni, B. Baeuerle, A. Josten, M. Zahner, U. Koch, Y. Salamin, C. Hoessbacher, C. Haffner, D. L. Elder, L. R. Dalton and J. Leuthod, "High-speed plasmonic modulator in a single metal layer," *Science*, vol. 358, no. 6363, pp. 630-632, 2017.
- [15] G. Ulliac, V. Calero, A. Ndao, F. Baida and M. P. Bernal, "Argon plasma inductively coupled plasma reactive ion etching study for smooth sidewall thin film lithium niobate waveguide application," *Optical Materials*, vol. 53, pp. 1-5, 2016.
- [16] N. Courjal, F. Devaux, A. Gerthoffer, C. Guyot, F. Henrot, A. Ndao and M. P. Bernal, "Low-loss LiNbO₃ tapered-ridge waveguides made by optical-grade dicing," *Optics Express*, vol. 23, no. 11, pp. 13983-13990, 2015.
- [17] P. O. Weigel and S. Mookherjea, "Reducing the thermal stress in a heterogeneous material stack for large-area hybrid optical silicon-lithium niobate waveguide micro-chips," *Optical Materials*, vol. 66, pp. 605-610, 2017.
- [18] J. L. Nightingale, R. A. Becker, P. C. Willis and J. S. Vrhel, "Characterization of frequency dispersion in Ti-indiffused lithium niobate optical devices," *Applied Physics Letters*, vol. 51, pp. 716-718, 1987.
- [19] Y. A. Vlasov and S. J. McNab, "Losses in single-mode silicon-on-insulator strip waveguides and bends," *Optics Express*, vol. 12, pp. 1622-1631, 2004.
- [20] P. O. Weigel, M. Savanier, C. T. DeRose, A. T. Pomerene, L. A. Starbuck, A. L. Lentine, V. Stenger and S. Mookherjea, "Lightwave Circuits in Lithium Niobate through Hybrid Waveguides with Silicon Photonics," *Scientific Reports*, 2016.
- [21] P. O. Weigel and S. Mookherjea, "Process Design Kit and Modulator Simulation for Hybrid Silicon-Lithium Niobate Integrated Optics," in Conference on Lasers and Electro-Optics (CLEO), San Jose, 2017, paper JTu5A.126.
- [22] D. M. Pozar, *Microwave Engineering*, Hoboken, NJ: Wiley, 2011.

- [23] G. Ghione, *Semiconductor Devices for High-Speed Optoelectronics*, Cambridge: Cambridge University Press, 2009.
- [24] G. E. Betts, "Microwave bandpass modulators in lithium niobate," *Integrated and Guided Wave Optics, 1989 Technical Digest Series*, vol. 4, pp. 14-17, 1989.
- [25] Y. Shi, L. Yan and A. E. Willner, "High-Speed Electrooptic Modulator Characterization Using Optical Spectrum Analysis," *Journal of Lightwave Technologies*, vol. 21, no. 10, pp. 2358-2367, 2003.
- [26] C. Hoessbacher, A. Josten, B. Baeuerle, Y. Fedoryshyn, H. Hettrich, Y. Salamin, W. Heni, C. Haffner, C. Kaiser, R. Schmid, D. L. Elder, D. Hillerkuss, M. Moller, L. R. Dalton and J. Leuthold, "Plasmonic modulator with >170 GHz bandwidth demonstrated at 100 GBd NRZ," *Optics Express*, vol. 25, pp. 1762-1768, 2017.
- [27] M. M. Howerton and W. K. Burns, "Broadband traveling wave modulators in LiNbO₃," in *RF Photonic Technology in Optical Fiber Links*, Cambridge University Press, 2002.
- [28] C. Haffner, W. Heni, Y. Fedoryshyn, J. Niegemann, A. Melikyan, D. L. Elder, B. Baeuerle, Y. Salamin, A. Josten, U. Koch, C. Hoessbacher, F. Ducry, L. Juchili, A. Emboras, D. Hillerkuss, M. Kohl, L. R. Dalton, C. Hafner and J. Leuthold, "All-plasmonic Mach-Zehnder modulator enabling optical high-speed communication at the microscale," *Nature Photonics*, vol. 9, pp. 525-528, 2015.
- [29] V. Sorianoello, M. Midrio, G. Contestabile, I. Asselberg, J. Van Campenhout, C. G. Huyghebaerts, A. K. Ott, A. C. Ferrari and M. Romagnoli, "Graphene-silicon phase modulators with gigahertz bandwidth," *Nature Photonics*, vol. 12, pp. 40-44, 2018.